Vol. 30 No. 129 *Journal of the Radio Research Laboratories* March 1983
Printed in Tokyo, Japan pp.59−87

COHERENCE LOSS AND DELAY OBSERVATION ERROR IN VERY-LONG-BASELINE INTERFEROMETRY

By
Noriyuki KAWAGUCHI

(Received on January 27, 1983)

CONTENTS

ABSTRACT

This paper reviews a signal-to-noise ratio (SNR) in Very-Long-Baseline Interferometry (VLBI). The SNR is an important factor to estimate a delay observation error and a formal error on solved-for parameters, such as baseline components, clock offsets and other physical quantities. The SNR is expressed as a function of system parameters, such as antenna gain, system noise temperature, video bandwidth and integration time, etc. Delay observation error is given in terms of the SNR and an "improvement factor" of bandwidth synthesis by taking coherence loss into account.

Consideration is paid for the coherence loss, i.e. deterioration of the SNR, by counting up every factor associated with that loss. Such factors include, not only the loss due to imperfection of a VLBI system, but also the loss due to phase fluctuations in atmosphere.

This paper gives the estimation of the loss caused in a K-3 VLBI system, i.e. Japanese VLBI system developed for Japan-US joint VLBI experiments starting early in 1984, and the estimation of the loss due to the phase fluctuations under the worst, the best and a typical weather conditions. The phase fluctuations under the typical weather condition is based on experimental results obtained by using a K-2 VLBI system, which is a real-time VLBI system developed before the K-3 system.

Finally, by taking the loss into acount, this paper gives the estimation of the delay

observation error in some concrete cases, such as 1) the Japan-US joint VLBI experiments between a 26-m antenna at Kashima, the Radio Research Laboratories, and a 40-m antenna in Owens Valley Radio Observatory, California, U.S.A., 2) domestic VLBI experiments between the 26-m antenna and a 5-m antenna at Tsukuba, Geographical Survey Institute, and 3) mobile VLBI experiments between the 26-m antenna and a transportable 3-m antenna.

1. Introduction

Delay in arrival time of a wavefront from an extra-galactic radio source at both ends of a baseline is one of the most important observables in Very-Long-Baseline Interferometry (VLBI)[1]. An error in measuring the delay is dependent on a signal-to-noise ratio (SNR), an improvement factor of bandwidth synthesis and a coherence loss.

In Chapter 2, a VLBI observation is briefly reviewed from the view point of signal-processing, and the SNR of one observation channel, i.e. an amplitude ratio of a correlated signal to uncorrelated noises in the channel, is defined by a function of system parameters, such as antenna gain, system noise temperature, correlated flux density of the radio source, video bandwidth and integration time. The delay observation error can be estimated from the SNR of one channel and an "improvement factor of bandwidth synthesis". The improvement factor defined in this paper gives a degree of improvement in delay observations where several frequency channels are synthesized with each other as compared with the case where only one channel is observed. The estimation is, however, an ideal case where no coherence loss accompanies the observations.

In Chapter 3, almost all loss factors found in an imperfect VLBI system are considered, and the estimation of the coherence loss is given for a K-3 VLBI system, a Japanese VLBI system developed for Japan-US joint VLBI experiments starting early in 1984[2].

In Chapter 4, consideration is given on the coherence loss due to phase fluctuations in atmosphere. And the estimation of the loss is given by using models for the worst, for the best and for a typical weather conditions. The model for the typical condition is based on the experimental results obtained by using a K-2 VLBI system[3], which is a real-time VLBI system developed before the K-3 system.

In Chapter 5, all he results are summarized, and the estimations of the delay observation error are given in the cases of some concrete VLBI experiments, such as 1) Japan-US joint VLBI experiments between a 26-m antenna in diameter at Kashima, the Radio Research Laboratories, Japan, and a 40-m antenna at Owens Valley Radio Observatory, one of the principal stations in a continental VLBI network in the U.S.A., 2) domestic VLBI experiments between the 26-m antenna and a 5-m antenna at Tsukuba, Geographical Survey Institute, Japan[4], and 3) future mobile-VLBI experiments between the 26-m antenna and a transportable 3-m antenna.

2. Signal-to-noise ratio (SNR) and delay observation error

2.1 Definition of SNR and delay observation error

Supposing the signal from an "unresolved" radio source arrives at one end of a baseline at time t, and comes late to another end at time $t + \tau_g$, we would observe $n_0(t)$ and its delayed replica $n_0(t - \tau_g)$ as a signal. By the word "unresolved" it is meant that the angular size of the radio source is much less than the fringe spacing λ/D_T, where D_T is the length of the baseline normal to the source direction, and λ is a wavelength. At each station, the signals coming through an aperture of the antenna are mixed with additive independent noises of n_1 (t) and n_2 (t) respectively. Then the observed signals are written as

$$s_1(t) = \sqrt{T_{a1}} \times n_0(t) + \sqrt{T_{s1}} \times n_1(t)$$
$$s_2(t) = \sqrt{T_{a2}} \times n_0(t-\tau_g) + \sqrt{T_{s2}} \times n_2(t), \quad \text{(2.1)}$$

where T_{a1}, T_{a2} are power density of the signals, given by[5]

$$T_{ai} = S_c A_{ei}/(2k)$$
$$= (\lambda^2/8\pi k)\, S_c G_i \,;\, i = 1, 2 \quad \text{(2.2)}$$

λ : wavelength
k : Boltzmann's constant (1.38 X 10^{-23} joule/deg)
A_{ei} : effective aperture of each antenna
S_c : correlated flux density of the radio source
G_i : antenna gain of each station

and T_{s1}, T_{s2} are power density of system noises. All of n_0, n_1, n_2 in Eq. (2.1) are normalized to unity in each power. If the source has some degree of polarization or has some angular extent, we must correct the Eq. (2.1) and Eq. (2.2) in exact forms, but here we assume the source is perfectly unresolved and unpolarized. The effect of the source extent and polarization would appear on the delay and the fringe-phase observations as systematic variations. This subject will be further discussed in other papers.

The observed signals, after frequency conversion, are sampled, recorded on tapes, reproduced, cross-correlated with each other and integrated. As a result of the processing, we obtain a cross-correlation function as

$$R_{12}(\tau_i) = \sqrt{T_{a1} T_{a2}}\, R_{00}(\tau_i - \tau_g) + \sqrt{T_{s1} T_{s2}}\, n_3(\tau_i), \quad \text{(2.3)}$$

where lags are numbered 1, . . . , i, . . . , K, and R_{00} (τ) is an auto-correlation function of n_0 (t); n_3 (τ_i) is a random variable generated from the n_1, n_2 by an equation

$$n_3(\tau_i) = (1/N) \sum_{j=1}^{N} n_1(t_j)\, n_2(t_j + \tau_i), \quad \text{(2.4)}$$

where n_1 (t_j), n_2 ($t_j + \tau_i$) are samples of n_1 (t) and n_2 (t) at t_j and $t_j + \tau_i$; N is the number of samples existing in an integration period of T. A square mean of the n_3 (τ_i) in Eq. (2.4) is

$$E[n_3(\tau_i)^2] = (1/N^2) \sum_{m=1}^{N} \sum_{n=1}^{N} E[n_1(t_m)\, n_2(t_m + \tau_i)\, n_1$$
$$(t_n)\, n_2(t_n + \tau_i)], \quad \text{(2.5)}$$

and if we assume that the n_1 (t) and n_2 (t) are independent of each other, and n_1 (t_m), n_2 ($t_m + \tau_i$) are independently sampled from n_1 (t), n_2 (t) respectively, Eq. (2.5) is expressed simply as (see Appendix)

$$E[n_3(\tau_i)^2] = 1/N \quad \text{(2.6)}$$

By Nyquist's theorem we can see that

$$N = 2BT, \qquad (2.7)$$

where signals of time duration T are sampled at the rate of 2B samples/sec after ideally low-pass filtered at a cutoff frequency of B Hz.

Introducing Eqs. (2.6) and (2.7) into (2.3) and normalizing the $n_3(\tau_i)$ to unity in its power, we obtain

$$R_{12}(\tau_i) = \sqrt{T_{a1}T_{a2}}\, R_{00}(\tau_i - \tau_g) + \sqrt{(T_{s1}T_{s2})/(2BT)}\, n_4(\tau_i), \qquad (2.8)$$

where $n_4(\tau_i)$ is a normalized version of $n_3(\tau_i)$. It is convenient and clear in physical meanings to define the signal-to-noise ratio (SNR) by the ratio of the correlated amplitude to the uncorrelated one. Since the correlated amplitude is $\sqrt{T_{a1}T_{a2}}$ and the uncorrelated one is $\sqrt{(T_{s1}T_{s2})/(2BT)}$ as seen in Eq. (2.8), the ratio can be written as

$$\mathrm{SNR} = \sqrt{(T_{a1}T_{a2})/(T_{s1}T_{s2}/2BT)} \qquad (2.9)$$

By using the SNR, Eq. (2.8) is rewritten as

$$R_{12}(\tau_i) = \sqrt{T_{a1}T_{a2}}\, [\, R_{00}(\tau_i - \tau_g) + (1/\mathrm{SNR})\, n_4(\tau_i)\,]. \qquad (2.10)$$

Now, we will proceed to the next discussion about a processing to determine the delay τ_g in Eq. (2.10). An ingenious way to determine the delay is to handle the cross-correlated data in frequency domain, namely to become a cross-spectrum, where a phase of the cross-spectrum is linearly changed with the frequency, and its slope gives us the fine delay τ_g.

The cross-correlation $R_{12}(\tau_i)$ is Fourie-transformed to the cross-spectrum $S_{12}(\omega_i)$ as

$$S_{12}(\omega_i) = (\sqrt{T_{a1}T_{a2}}/K)\, [\exp(j\omega_i\tau_g) + r_i \exp(j\theta_i)]. \qquad (2.11)$$

Since the second term in the square bracket is a Fourier-transform of a band-limited Gaussian noise $n_4(\tau_i)$, the amplitude r_i has a Rayleigh probability distribution with a variance of σ_ϵ^2 as

$$p(r_i) = (r_i/\sigma_\epsilon^2)\exp(-r_i^2/2\sigma_\epsilon^2), \qquad (2.12)$$

whereas the phase θ_i is uniformly distributed over the range 2π.

Since the noise power in time domain ($T_{a1}T_{a2}/\mathrm{SNR}^2$ from Eq. (2.10)) should be equal to that in frequency domain, the variance in Eq. (2.12) is determined as follows:

From Eq. (2.11), the noise power in frequency domain is

$$\sum_{i=1}^{K} E\,[(T_{a1}T_{a2}/K^2)\, r_i^2\,] = (T_{a1}T_{a2}/K^2)\sum_{i=1}^{K}\int_0^\infty r_i^2\, p(r_i)\, dr_i,$$

and from Eq. (2.12),

$$= (2T_{a1}T_{a2}/K)\cdot\sigma_\epsilon^2,$$

and should be

$$= (T_{a1}T_{a2}/\mathrm{SNR}^2)$$

Consequently, σ_ϵ^2 in Eq. (2.12) becomes

$$\sigma_\epsilon^2 = (K/2)(1/SNR^2) \quad \ldots\ldots (2.13)$$

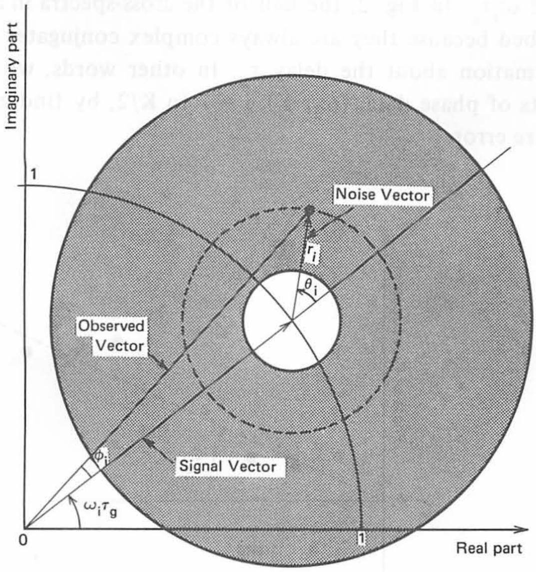

Fig. 1 Phase error of the cross-spectrum observed at a specific frequency component around a true phase of $\omega_i\tau_g$ The 80% of noises may be realized within a shaded part bordered by two circles, while the maximum probable occurrences are on a broken circle when the SNR is 6.

Since the S_{12} (ω_i) is composed of signal $\exp(j\omega_i\tau_g)$ and noise $r_i \exp(j\theta_i)$ as shown in Eq. (2.11), the observed phase of cross-spectrum, ϕ_i, would be realized around a true phase of $\omega_i\tau_g$ as shown in Fig. 1. The probability distribution of the resultant phase, ϕ_i, is given as follows[6]:

$$p(\phi_i) = (1/2\pi)\exp(-1/2\sigma_\epsilon^2)\left\{1 + \sqrt{\pi/2}\,(\cos(\phi_i - \omega_i\tau_g)/\sigma_\epsilon) \times \exp[\cos^2(\phi_i - \omega_i\tau_g)/2\sigma_\epsilon^2]\cdot[1 + \mathrm{erf}(\cos(\phi_i - \omega_i\tau_g)/\sqrt{2}\sigma_\epsilon]\right\}, \quad \ldots\ldots (2.14)$$

where erf (x) is the error function given by

$$\mathrm{erf}(x) = 2/\sqrt{\pi}\int_0^\infty \exp(-\phi^2)\,d\phi \quad \ldots\ldots (2.15)$$

If σ_ϵ is much less than unity (as in usual cases), Eq. (2.14) is well approximated by a simple Gaussian distribution as

$$p(\phi_i) = (1/\sqrt{2\pi}\sigma_\epsilon)\exp[-(\phi_i - \omega_i\tau_g)^2/2\sigma_\epsilon^2]. \quad \ldots\ldots (2.16)$$

Thus standard deviations of the observed phases around a true phase of $\omega_i\tau_g$ are equal to σ_ϵ expressed in Eq. (2.13).

A similar discussion holds for any other frequency components, so observed phases of the cross-spectrum may be realized as shown in Fig. 2, where each phase has a standard deviation of σ_ϵ around $\omega_i\tau_g$. In Fig. 2, the half of the cross-spectra in a negative frequency domain are not described because they are always complex conjugates of positive half and do not give any information about the delay τ_g. In other words, we should estimate the delay τ_g from K/2 sets of phase data, (ω_i, ϕ_i), i = 1 to K/2, by finding the slope of them which minimize a square error.

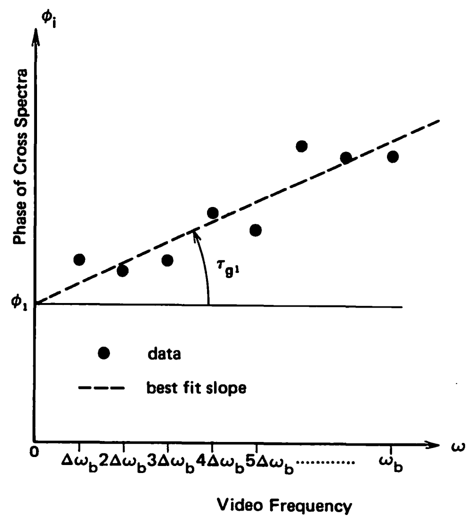

Fig. 2 Example of the phases of the cross-spectrum
The slope of phase spectra (filled circles) in one video channel gives the delay in arrival time of wave front at each station.

Using the least square method, the most likely estimate of the τ_g, which we denote as $\hat{\tau}_{g1}$, is given by

$$\hat{\tau}_{g1} = [K'(\sum_i \omega_i\phi_i) - (\sum_i \omega_i)(\sum_i \phi_i)]/[K'(\sum_i \omega_i^2) - (\sum_i \omega_i)^2], \quad \text{.............. (2.17)}$$

where the summation, $\sum_i$, are understood to run from i = 0 to i = K'-1, and K' is the number of independent frequency components, i.e., the half of independent time data,

$$K' = K/2. \quad \text{.. (2.18)}$$

As derived in the paper(7), the variance of τ_{g1}, $\sigma_{\tau 1}{}^2$, is calculated to be

$$\sigma_{\tau 1}{}^2 = K'\sigma_\epsilon{}^2/[K'(\sum_i \omega_i)^2 - (\sum_i \omega_i)^2], \quad \text{............................ (2.19)}$$

where all the variances of ϕ_i are equal to $\sigma_\epsilon{}^2$, which was expressed by a function of the SNR in Eq. (2.13).

On the other hand, the most likely estimate of a fringe phase, $\hat{\phi}_1$, is an average of ϕ_i as

$$\hat{\phi}_1 = (1/K') \sum_i \phi_i, \quad \ldots \quad (2.20)$$

which represents the most likely phase at a mean frequency of

$$\bar{\omega} = (1/K') \sum_i \omega_i, \quad \ldots \quad (2.21)$$

and the variance of $\hat{\phi}_1$ is

$$\sigma_{\phi 1}{}^2 = \sum_i \left(\frac{\partial \hat{\phi}_1}{\partial \phi_i}\right)^2 \sigma_\epsilon{}^2$$

$$= \sigma_\epsilon{}^2/K', \quad \ldots \quad (2.22)$$

where $\frac{\partial \hat{\phi}_1}{\partial \phi_i}$ is a partial derivative of $\hat{\phi}_1$ with respect to ϕ_i and easily calculated by using Eq. (2.20). Substituting Eqs. (2.13) and (2.18) for $\sigma_\epsilon{}^2$ and K' in this equation, we get the following relationship of $\sigma_{\phi_1}{}^2$ with the SNR as

$$\sigma_{\phi 1}{}^2 = (1/\mathrm{SNR})^2 \quad \ldots \quad (2.23)$$

In the meantime, since phase spectra in number K' are arranged with separation of equal distances $\Delta\omega_b$, in a frequency band from 0 to ω_b, we can write ω_i in Eq. (2.19) by

$$\omega_i = i\Delta\omega_b \;\; ; \Delta\omega_b = \omega_b/K'$$

$$; i = 0 \text{ to } K' - 1 \quad \ldots \quad (2.24)$$

Introducing this into Eq. (2.19) and performing the summations, we get the following expression for σ_{τ_1}.

$$\sigma_{\tau 1}{}^2 = (12\,\sigma_\epsilon{}^2/\omega_b{}^2)\,[K'/(K' - 1)(K' + 1)] \ldots \quad (2.25)$$

Again substituting Eqs. (2.13) and (2.18) into this equation, this becomes

$$\sigma_{\tau 1}{}^2 = [12/(\omega_b \mathrm{SNR})^2]\;[K'^2/(K' - 1)(K' + 1)], \quad \ldots \quad (2.26)$$

and from the fact that a value in the second square bracket is almost equal to unity for all K' greater than 2, this can be approximately reduced to

$$\sigma_{\tau 1}{}^2 = 12/(\omega_b \mathrm{SNR})^2. \quad \ldots \quad (2.27)$$

Eq. (2.27) is a conclusion of this section and it defines the relation between delay observation error and system parameters through the SNR.

2.2 Improvement of delay observation error by a bandwidth synthesis method

According to the studies made so far, it is concluded that the delay observation error and the phase observation error are inversely proportional to the SNR and are related to the system parameters through Eqs. (2.9) and (2.2). It can also be seen that a wider bandwidth results in the better SNR and better observations. The bandwidth is, however, limited to only a few MHz for one receiving channel by the limitation of video-converting, sampling, recording and processing. Thus a bandwidth synthesis method has been developed by Rogers[8] to improve the delay observation error remarkably. In this method, several channels, each of which has bandwidth of ω_b, are widely deployed over several hundred MHz, namely, the utmost extent of the receiver bandwidth, and are synthesized to each other as shown in Fig. 3. Each point in the figure represents the fringe phase observed at each channel and has the standard deviation of the phase observation error, σ_{ϕ_1}, which has already been studied and given in Eq. (2.23).

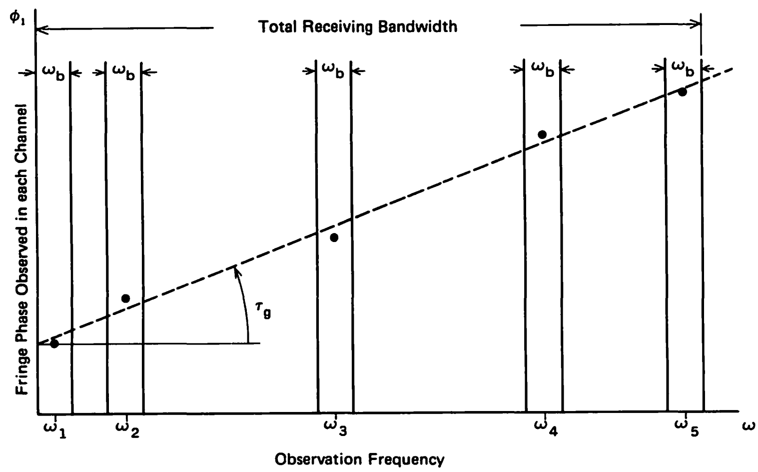

Fig. 3 Improvement of the delay observation error by means of bandwidth synthesis
Fringe phases (filled circles) determined in each video channel are synthesized with each other and the resultant slope gives the delay improved in the accuracy.

To obtain the estimate of the delay observation error after synthesizing these channels, again the least square method is used. The most likely estimate of the delay τ_g, i.e. a bandwidth-synthesized delay which we will denote as $\hat{\tau}_g$, is expressed by the same form of equation as Eq. (2.17) if replacing $\hat{\tau}_{g1}$ with $\hat{\tau}_g$, ϕ_i with $\hat{\phi}_1$ of each channel and K′ with M, which is the number of channels. The variance of the $\hat{\tau}_g$ is also calculated by the same form of equation as Eq. (2.19),

$$\sigma_\tau^2 = M\sigma_{\phi 1}^2 / [M(\Sigma\omega_i^2) - (\sum_i \omega_i)^2], \quad \ldots\ldots (2.29)$$

where, in this case, ω_i (i = 1 to i = M) is frequency allocated to each channel which is not always arranged at equal frequency distance. So it is convenient to define the RMS scattering of the observation frequencies, ω_{rms} as

$$\omega_{rms} = \sqrt{(1/M)\sum_i(\omega_i - \bar{\omega})^2}\ ;\ \bar{\omega} = (1/M)\sum_i \omega_i, \quad \ldots\ldots (2.30)$$

and then Eq. (2.29) becomes

$$\begin{aligned}\sigma_\tau^2 &= \sigma_{\phi 1}^2/(M\omega_{rms}^2)\\ &= 1/(M\omega_{rms}^2\ SNR^2). \quad \ldots\ldots (2.31)\end{aligned}$$

According to this and Eq. (2.27), it is obvious that the delay observation error is improved as compared with the case of only one channel by a factor of η given by

$$\eta = \sqrt{12M}\,(\omega_{rms}/\omega_b) \quad \text{(2.32)}$$

and $$\sigma_T = \sigma_{T1}/\eta. \quad \text{(2.33)}$$

We will call η an "improvement factor" by the bandwidth synthesis method.

It is worth while to note that the σ_{T_1} is dependent on the SNR and the system parameters in the last analysis, while the η is not dependent on the system parameters but only on the arrangement of channels. From Eq. (2.32), it can easily be seen that when the system parameters are the same, the maximum frequency scattering, max ω_{rms}, gives the maximum improvement in delay observations. On the occasion of planning an arrangement of observation channels, however, another factor should be considered as well, which is a delay ambiguity defined by a reciprocal of the maximum greatest common measure in observation frequencies, and this subject is further discussed in the other papers[9][10].

Anyway, the delay observation error depends on system parameters and an arrangement of observing channels, and here the relations required in the estimation of the delay observation error are summarized as follows:

$$\sigma_T = \sigma_{T1}/\eta$$
$$\eta = \sqrt{12M}\,(\omega_{rms}/\omega_b)$$
$$\sigma_{T1} = \sqrt{12}/(\omega_b \mathrm{SNR})$$
$$\mathrm{SNR} = \sqrt{(2BT\,T_{a1}T_{a2})/(T_{s1}T_{s2})}$$
$$T_{ai} = (\lambda^2/8\pi k)\,S_c G_i$$
$$\omega_b = 2\pi B$$

where

σ_T : delay observation error after bandwidth synthesizing
η : improvement factor by bandwidth synthesis
σ_{T1} : delay observation error in a specific channel
M : number of channels to be synthesized
ω_{rms} : rms scattering of the observation frequencies
ω_b : angular frequency bandwidth of one channel
SNR : signal-to-noise ratio, a ratio of correlated amplitude to uncorrelated one
B : bandwidth of one channel (Hz)
T : integration time (sec)
T_{ai} : power density of signal obtained by receiving a radio source (Kelvin)
T_{si} : power density of system noise (Kelvin)
λ : observation wavelength (meter)
S_c : correlated flux density of the radio source (watt/m^2/Hz)
G_i : : antenna gain
k : Boltzmann's constant (1.38×10^{-23} joule/deg)

3. Coherence loss due to system imperfectness

In the preceding section, the estimation of the delay observation error is mentioned in such an ideal case as perfect receiving and filtering, flawless sampling of signals and ideal data processing. If the receiving and prcessing system is not perfect, however, some amount of the correlated power is lost in the system, and as a result of that, we will suffer the deterioration of the SNR, in other words, the loss of coherence.

In this section, every loss factor caused by the imperfect system is counted up, and the estimations of the losses are given.

3.1 Imperfect receiving

The noise generated in a receiver has been already considered, but in the consideration, the ideal frequency conversion is assumed. The n_0 (t) in Eq. (2.1) has been the video signal perfectly converted in frequency from the radio band to the video band with phase information perfectly maintained. In a usual case, however, a local oscillator has more or less frequency instability, and the resultant phase fluctuation on the video signal causes the coherence loss.

If the phase fluctuation is denoted by φ (t), the cross spectrum S_{12} (ω_i) in Eq. (2.11) becomes

$$S_{12}'(\omega_i) = S_{12}(\omega_i) \exp[j\varphi(t)], \qquad (3.1)$$

and it is convenient to define a coherence loss function as

$$C(T) = |(1/T)\int_0^t \exp[j\varphi(t)]\, dt|, \qquad (3.2)$$

where C (T) expresses the diminution from the unity due to incoherent averaging for integration period of T.

As is derived in the reference(11), the square mean of the C (T) can be expressed in terms of the statistics commonly used in the field of frequency standards as

$$E[C^2(T)] = (2/T)\int_0^t \exp[-\omega_0{}^2\tau^2 I^2(\tau)/2]\,(1-\tau/T)\, d\tau, \qquad (3.3)$$

where I^2 (τ) denotes a "true variance", a measure of instantaneous frequency instability defined by

$$\begin{aligned} I^2(\tau) &= E\left\{([\varphi(t_k+\tau)-\varphi(t_k)]\,/\,\omega_0\tau)^2\right\} \\ &= E[\bar{y}_\tau{}^2], \end{aligned} \qquad (3.4)$$

which is a theoretical idealization(11).

It is often convenient to use an Allan variance, $\sigma_y{}^2$ (τ), instead of the true variance, I^2 (τ), for a practical reason that the frequency instability needs to be estimated with a finite number of samples. So the problem is to make clear the relation between the true variance and the Allan variance, and the answer is partly given in the reference(11) in the special case of white phase noise and white frequency noise.

For white phase noise, we get the relation

$$\begin{aligned} I^2(\tau) &= (2/3)\,\sigma_y{}^2(\tau) \\ &= (2/3)\,\alpha_p\tau^{-2}, \end{aligned} \qquad (3.5)$$

where α_p is the Allan variance of white phase noise at averaging time of 1 second, and for white frequency noise

$$\begin{aligned} I^2(\tau) &= \sigma_y{}^2(\tau) \\ &= \alpha_f \tau^{-1}, \qquad \text{(3.6)} \end{aligned}$$

where α_f is the Allan variance of white frequency noise at averaging time of 1 second.

Substituting Eqs. (3.5) and (3.6) into (3.3), and carrying out the integration, the coherence loss, L_c, is given in the cases of these two kinds of noise as

$$\begin{aligned} L_c &= 1 - \sqrt{E[C^2(T)]} && \text{(3.7)} \\ &= \alpha_p \omega_0{}^2/6 \quad \text{; for white phase noise} && \text{(3.8)} \\ &= \alpha_f T \omega_0{}^2/12 \quad \text{; for white frequency noise} && \text{(3.9)} \end{aligned}$$

In addition to these two kinds of noise, it is well known that there is another kind of noise, Flicker frequency noise, in a typical frequency standard. To obtain the estimation of the loss due to the Flicker frequency noise, we must start to review a general relationship between $I^2(\tau)$ and $\sigma_y{}^2(\tau)$[12], which is given by

$$\sigma_y{}^2(\tau) = 2\,[I^2(\tau) - I^2(2\tau)]. \qquad \text{(3.10)}$$

In the cases of white phase noise and white frequency noise, this formula has already been solved for $I^2(\tau)$[11] as

$$2I^2(\tau) = \sigma_y{}^2(\tau) + \sigma_y{}^2(2\tau) + \sigma_y{}^2(4\tau) + \ldots\ldots, \qquad \text{(3.11)}$$

where $I^2(\tau)$ converges to a finite value as already shown in Eqs. (3.5) and (3.6). In the case of the Flicker frequency noise, however, the true variance $I^2(\tau)$ goes to infinity, because the Allan variance is always constant, i.e.

$$\begin{aligned} \sigma_y{}^2(\tau) &= \sigma_y{}^2(2\tau) = \sigma_y{}^2(4\tau) = \ldots\ldots \\ &= \sigma_y{}^2. \qquad \text{(3.12)} \end{aligned}$$

This difficulty has been pointed out in the reference[11] and is solved by taking a filtering effect of "fringe search" processing into account. Here, another solution of Eq. (3.10) for $I^2(\tau)$ is presented as

$$I^2(\tau) = (\sigma_y{}^2/2\ln 2)\ln(\tau_{max}/\tau), \qquad \text{(3.13)}$$

where τ_{max} is an arbitrary constant of sufficiently large value.

It can easily be proved that Eq. (3.13) also satisfies Eq. (3.10) for the constant Allan variance, but the solution has the arbitrary parameter, τ_{max} which should be fixed by introducing another condition.

Consider again the "fringe search" processing discussed in the reference[11], which is a common technique in VLBI data processing. In the procedure, the most fitted fringe frequency is searched for the maximum value of C (T). The processing may be interpreted as a kind of filtering, but more exactly speaking, the processing should be understood as the removal of the linear phase drift, in other words, the removal of a mean frequency offset over the coherent integration. Thus the true variance for the averaging time of T is forced to be zero, that is

$$I^2(T) = 0 \qquad (3.14)$$

Introducing this condition into Eq. (3.13), we get the relation between the true variance and the constant Allan variance of Flicker frequency noise as

$$I^2(\tau) = (\sigma_y{}^2/2\ln 2)\ \ln(T/\tau) \qquad (3.15)$$

Substituting this into Eq. (3.3), giving an approximation of $\exp(-x^2)$ to $(1-x^2)$ and carrying out the integration, we get the estimate of the coherence loss owing to Flicker frequency noise as

$$L_c = \omega_0{}^2\sigma_y{}^2T^2/57 \qquad (3.16)$$

By bringing all the results over a conclusion, we get the following equation useful to estimate the coherence loss due to imperfect receiving, in other words, due to the instability of frequency standard:

$$L_c = \omega_0{}^2\ (\alpha_p/6 + \alpha_f T/12 + \sigma_y{}^2 T^2/57) \qquad (3.17)$$

ω_0 : angular frequency of a local oscillator (rad/sec)
α_p : Allan variance of white phase noise at 1 sec
α_f : Allan variance of white frequency noise at 1 sec
$\sigma_y{}^2$: constant Allan variance of Flicker frequency noise
T : integration time (sec)

3.2 Imperfect image rejection

In radio interferometry, observation-frequency windows are transferred down to a video channel by one or more single-sideband conversions. Usually, the first conversion is from the radio frequencies to the intermediate frequencies, and the second is from the intermediate frequencies to the video frequencies. For the second conversion, an image-rejection mixer is often used in a modern VLBI system. The mixer separately converts the upper and lower sidebands around a local frequency into two video channels as suggested in Fig. 4. The 90-deg phase-difference networks in the mixer play an important role in the separation of the upper sideband from the lower one, and vice versa. Especially, the network operating at video frequencies primarily determines the performance of an image rejection ratio and is required to cover decades of bandwidth, say from several hundred Hz to several MHz.

The image rejection ratio can easily be measured by using a white-noise generator and a correlation processor as illustrated in Fig. 5, and is given by

$$\beta_{ir} = [1 - \sqrt{1-(2r)^2}\,]/(2r), \qquad (3.18)$$

where $$r = R_{UL}/(R_{UU} + R_{LL}), \qquad (3.19)$$

and R_{UL} is the measured cross-correlation value between the upper and lower sidebands and each of R_{UU} and R_{LL} is the measured auto-correlation value of each sideband.

Signals coming from unwanted sideband disappear in the course of fringe-rotation process, because the phase of unwanted sideband rotate in opposite direction to those of the desired ones and cannot be tracked along with the fringe-rotation compensation described in

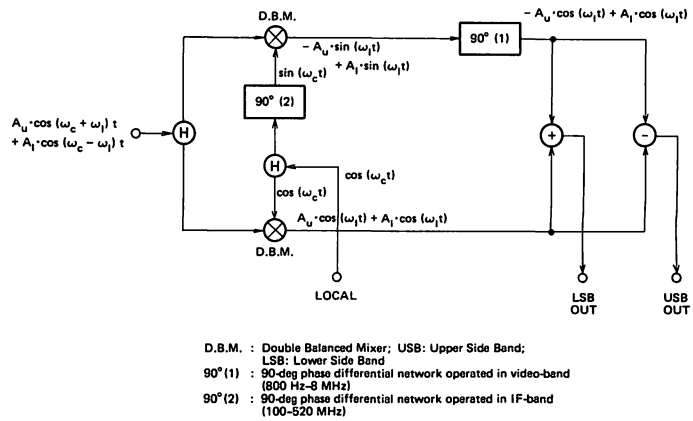

Fig. 4 Conceptional block diagram of the image rejection mixer with two 90-deg phase difference networks

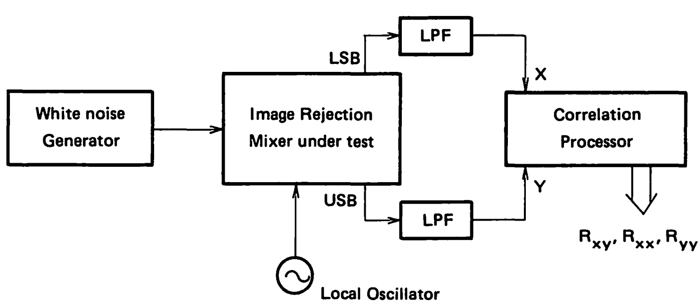

Fig. 5 Evaluation of the image rejection ratio by using a white noise generator and a correlation processor

Section 3.6. On the other hand, signals going away from the desired sideband decrease the power available for the desired channel. This causes the loss of coherence which is directly related to the image rejection ratio given by Eq. (3.18).

3.3 Imperfect filtering[13]

There are two loss factors which result from using a bandpass filter which is not perfectly rectangular in shape. The first is due to aliasing or foldover of noise from frequencies above the bandedge ω_b, while the second is due to the statistical dependence of one sample upon the following samples.

The first loss factor is given by

$$\beta_F = \int_0^{\omega_b} P(\omega)\, d\omega \Big/ \int_0^{2\omega_b} P(\omega)\, d\omega_b, \qquad (3.20)$$

where P (ω) is a power response of a bandpass filter. According to Fig. 6, it is obvious that the effect of the aliasing decreases as a cut-off frequency of the filter becomes lower than the bandedge ω_b, whereas the low cut-off frequency increases in statistical dependence between samples.

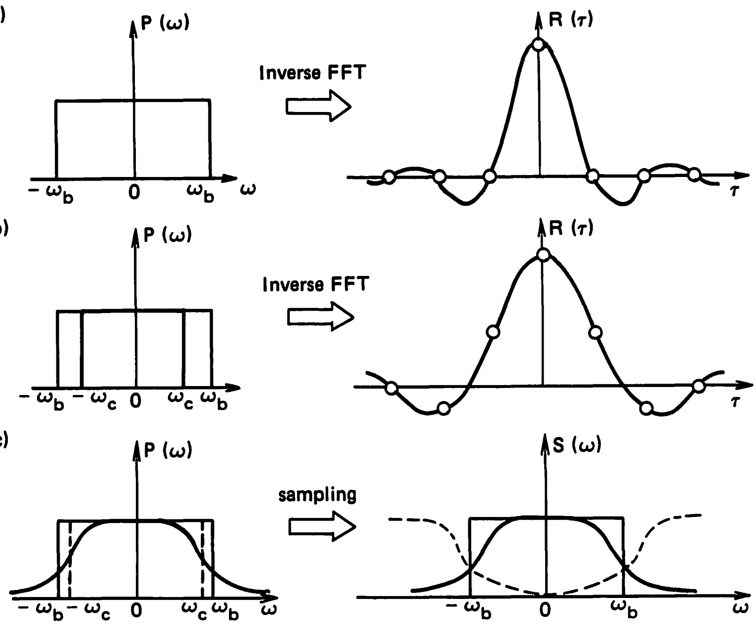

Fig. 6 Coherence loss associated with imperfect filtering
(a) If a low pass filter with cut-off frequency of ω_c has an ideal rectangular shape in the frequency response and data are sampled at frequency of ω_b, no coherence loss arises.
(b) If the cut-off frequency (ω_c) is lower than the sampling frequency (ω_b), samples shown by open circles are statistically dependent on others and coherence loss arises. The loss is increased as the cut-off frequency becomes lower and lower.
(c) Frequency components above sampling frequency (ω_b) are folded into a video channel and they works as noise. So the SNR in the channel is deteriorated and the deterioration can be interpreted as coherence loss. The loss is decreased as the cut-off frequency becomes lower and lower.

The second loss factor is associated with the statistical dependence. In Eq. (2.6), we assumed the statistical independence between samples, but if the correlation between samples is not zero, we must modify the equation in an exact form as

$$E\,[n_3\,(\tau_i)^2\,] = (1/N)\,[1 + 2\sum_{\tau=1}^{N} R_{11}\,(\tau)\,R_{22}\,(\tau)]\,, \qquad (3.21)$$

where R_{11}, R_{22} are auto-correlation functions of n_1 (t) and n_2 (t) respectively (see Appendix). These are reverse Fourie trasnformation of the power response of filters, P (ω), used in each station.

Eq. (3.21) means that the noise power is increased by a factor of $[1 + 2 \sum_{\tau=1}^{N} R_{11}(\tau) R_{22}(\tau)]$ as compared with Eq. (2.6). Hence, the coherence loss due to statistical dependence between samples, deterioration of the SNR, is given by

$$\beta_R = 1/\sqrt{1 + 2 \sum_{\tau=1}^{N} R_{11}(\tau) R_{22}(\tau)} \quad \ldots\ldots (3.22)$$

As discussed before, the low frequency cut-off of a filter results in small β_R but large β_F, there must be an optimum cut-off frequency which maximizes $\beta_F \beta_R$. In Table 1, the total loss due to imperfect filtering, β_f (= $\beta_R \beta_F$), optimized in the cut-off frequency, is given according to several orders of a Butterworth-type filter.

Table 1 Total losses due to imperfect filtering by Butterworth low pass filters after optimizing in their cut-off frequencies

No. of poles of Butterworth filter	Optimum cut-off frequency	foldover loss $1 - \beta_F$ in percent	loss due to statistical dependence $1 - \beta_R$ in percent	Total loss $1 - \beta_F \beta_R$ in percent
2	0.67	7	5	12
3	0.79	5	3	8
4	0.80	3	3	6
5	0.88	3	2	5
6	0.90	3	1	4
7	0.91	2	1	3
9	0.96	2	0.3	2.3
15	0.96	1	0.5	1.5

3.4 Clipping of a video signal

From the discussion in Section 2, the most important information in VLBI is a phase of a video signal and not an amplitude of that. Hence adoption of digital recording system is main current in recent VLBI observations, where the video signal is clipped, keeping only information about the zero-crossing, and then the clipped waveform is sampled at a constant rate. This method decreases not only a volume of data but also makes the correlation process simple. However, some coherence loss inevitably accompany the clipping and quantizing in one bit.

The effect of the clipping has been analyzed by several authors and summarized in the reference(14), and the loss due to the one-bit clipping, β_q, has been given as

$$\beta_q = 2/\pi \quad \ldots\ldots (3.23)$$

This is derived from theoretical idealization of the clipping, assuming that s (t_i) is equal to "1" if s (t_i) is greater than zero and equal to "0" if it is less than zero.

An actual device for clipping, however, has always some range around zero where it cannot detect the change of sign of the voltage. This means that some data around zero are of no use to find out the phase of the signal.

As it can be assumed that the video signal is a Gaussian noise, the loss due to the imperfect clipping can be written as

$$\beta_c = \sqrt{2/\pi}\int_{x_{min}}^{\infty} \exp(-x^2/2)\,dx, \quad \ldots\ldots (3.24)$$

where $x_{min} = V_{min}/V_{rms}$; V_{min} is the minimum detectable voltage of the device and V_{rms} is the rms voltage of the video signal. As can be seen from the equation, we can reduce the loss by increasing V_{rms}, that is, by using a video amplifier with sufficiently higher gain. A recent VLBI system allows only one percent loss at most.

3.5 Imperfect data recording and reproducing

In the course of data recording and reproducing, some amount of information is lost owing to misidentification of data bits, which is checked by a parity bit included in a byte (one byte is composed of eight bits).

If we express parity error rate by P_E, the loss is given by the following equation

$$\beta_{PER} = 1 - 7P_E \quad \ldots\ldots (3.25)$$

in the worst case, because if one parity error occurs, there is possibility that all seven bits in the byte are misunderstood.

The P_E varies with weariness of magnetic heads, adjustment of recording and reproducing electronics, and coercivity of a magnetic tape used, but is usually guaranteed to be less than one part of 10^3. Hence it is enough for us to take the loss factor of 0.99 into account.

3.6 Loss in correlation processing

In order to alleviate load of computer working for data reduction, cross-correlation and integration are recently carried out by a correlation processor. Owing to some limitation in the correlation processor, however, two kinds of loss accompany the processing, such as a fringe-rotation compensation and a fractional bit correction.

The most common technique to compensate the fringe rotation is to multiply the cross-correlation function by exp $(j\omega_f t)$, where ω_f is a frequency of the fringe rotation. In multiplying, however, we need to use so many complicated circuits that we usually make an approximation of exp $(j\omega_f t)$ with a function having only three values of "1", "0", "−1", denoted by C (t) + jS (t) as illustrated in Fig. 7. The first loss is due to this approximation and is discussed in the following.

It is easily derived that the function, C (t) + jS (t), is expanded in a Fourie series as

$$C(t) + jS(t) = \sum_{m=0}^{\infty} \gamma_m \exp[j(-1)^m (2m+1)\,\omega_f t], \quad \ldots\ldots (3.26)$$

where

$$\gamma_m = [4/\pi)/(2m+1)] \cos[(2m+1)\,\pi/8]. \quad \ldots\ldots (3.27)$$

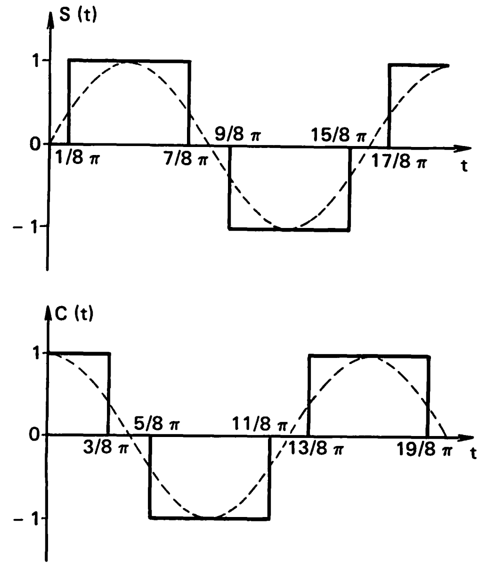

Fig. 7 Approximation of sine and cosine function with S (t) and C (t)

Only the first term of the series works for compensation of the fringe rotation, and the others disperse the correlated power. Hence the ratio of the amplitude of the first term to the root-sum-squares of all terms shows a loss of coherence due to the approximation, which is expressed as

$$\beta_{fr} = \gamma_0 / \sqrt{\Sigma |\gamma_m|^2} \quad \text{(3.28)}$$

Substituting Eq. (3.27) into (3.28), we get

$$\beta_{fr} = 2/3\ (4/\pi) \cos(\pi/8) = 0.960 \quad \text{(3.29)}$$

Here it should be noted that the three-level approximation yields the loss of 4% as seen in Eq. (3.29), but makes the multiplying remarkably simple, where the multiplying by "1" is equivalent to do nothing, the multiplying by "0" is to stop the integration, and the multiplying by "−1" is only to change a bit.

Another loss is due to discontinuous tracking of a delay change, that is to say, the loss due to a fractional bit, β_{fb}, as suggested in Fig. 8. As illustrated by solid lines in the figure, the simplest way to track the delay change is to shift data in a register by one bit after the delay change corresponding to one bit has occurred. This is the case where fractional bit correction is not performed.

By the aid of Fig. 9, it is obvious that the loss due to this simple delay tracking can be expressed as

$$\beta_{fb} = (1/B \times T_{FB}) \int_0^B \int_0^{T_{FB}} \cos[2\pi(f - B/2)\dot{\tau}_g t]\, dt df, \quad \text{(3.30)}$$

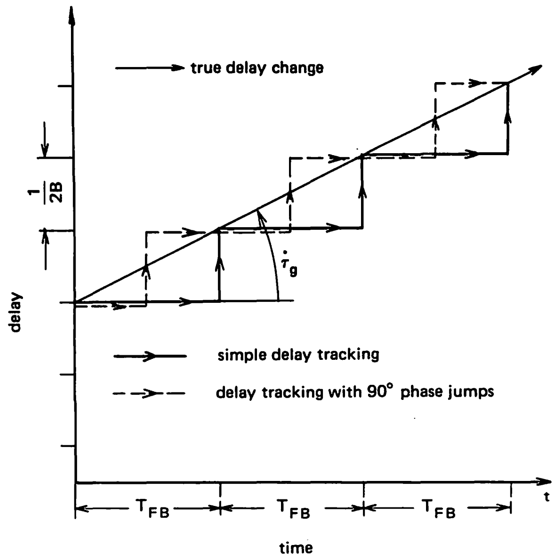

Fig. 8 Discontinuous tracking of a delay change

where B is a video bandwidth in Hz, f denotes a frequency in the video band, $\dot{\tau}_g$ is a delay rate and T_{FB} is a time required for the change of delay by one bit, which can be written as

$$T_{FB} = 1/(2B\dot{\tau}_g). \qquad (3.31)$$

Introducing this into Eq. (3.30) and performing the integration, we get the loss factor of 0.87 for β_{fb}. This means that 13% of coherence are lost in the case of no fractional bit correction.

Although perfect correction is to multiply the cross-spectrum by exp $[-\,j2\pi\,(f - B/2)\,\dot{\tau}_g t]$, it is very difficult to do and is even impossible to do in the time domain. Thus a skillful method for the cross-correlation processor operating in the time domain is devised(15).

This delay-tracking method is illustrated in Fig. 8 by dashes, where bit shifts are carried out at a time when a half bit of delay has changed. This method requires a 90-deg phase jump simultaneously with the bit shifts as suggested in Fig. 10, but reduces the maximum phase deviation to a half of that in case of the simple delay tracking. Hence β_{fb} in Eq. (3.30) becomes as

$$\beta_{fb} = (1/B \times T_{FB}) \int_0^B \int_0^{T_{FB}} \cos\,[\pi\,(f - B/2)\,\dot{\tau}_g t]\ dtdf, \qquad (3.32)$$

and again introducing Eq. (3.31) into this equation, we get 0.966 for β_{fb}. This corresponds to loss of 3.4% and is much smaller than that of 13% in the case of simple delay tracking.

3.7 Summary of loss factors due to system imperfectness

In this section, we will give a summary of loss factors due to system imperfectness discussed in the previous sections and give the estimation of the loss on the assumption that a K-3 VLBI system(2) is used in VLBI observations.

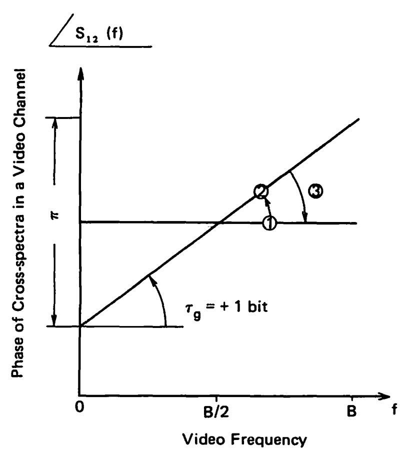

Fig. 9 Phase variation of frequency spectra in a video channel with time when delay changes are tracked by the simple method.
1 Start
2 One-bit tracking error occurs.
3 One-bit is shifted to track the delay change.

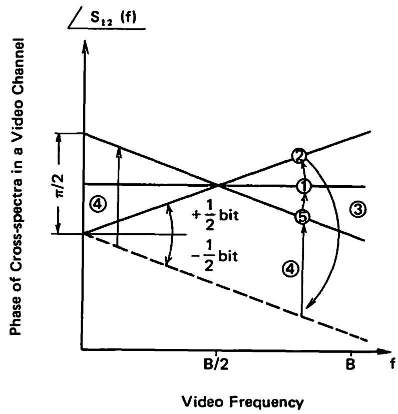

Fig. 10 Phase variation of frequency spectra in a video channel with time when delay changes are tracked by one-bit shift with 90° phase jump at a time when a half-bit delay has changed
1 Start
2 Half-bit tracking error occurs.
3 One-bit is shifted.
4 90-deg phase jump
5 Half-bit is advanced.

The following assumptions are made in the estimation: 1) S- and X-band signals are received, the center frequencies of which are 2270 MHz and 8390 MHz respectively, and 2) hydrogen maser oscillators generate reference signals of local oscillators for frequency conversion, the frequency instability of which has been measured on maser oscillators developed by the Radio Research Laboratories and the instability factors included in Eq. (3.17) are given as

$$\alpha_p = 1.0 \times 10^{-26}$$
$$\alpha_f = 5.0 \times 10^{-27}$$
$$\sigma_y = 3.0 \times 10^{-29} \qquad (3.33)$$

and 3) the integration time is 1000 seconds.

Introducing these values into Eq. (3.17), we get the loss of 0.6% due to imperfect receiving in X-band. Because the integration time of 1000 seconds is rather long as compared with usual observation time and, of course, the loss in S-band is much less than that in X-band, we can conclude that the loss of 0.6% is the value for the worst case and occupies a minority of the total loss.

In video converters included in the K-3 VLBI system, image-rejection mixers with broadband 90-deg phase difference networks[16] are used. They have a superior performance in the image rejection of far less than −20 dB. The image rejection ratio has been measured by using a method suggested in Section 3.2, and found to be −26 dB. This is equivalent to the loss of 0.5% due to imperfect image rejection.

The low-pass filters in the video converters are those of Butterworth type with seven poles in their transfer functions and are optimized in their cut-off frequencies as discussed in Section 3.3. As can be seen in Table 1, the loss due to imperfect fitering by these filters are estimated to be about 3%.

The loss due to the clipping has been discussed in Section 3.4 and estimated to be 36% by Eq. (3.23). This occupies a majority of the total loss and is desired to be improved. For the improvement, we need to make a drastic reformation of the current VLBI system, e.g. adoption of multi-bit sampling system, which should be realized in future. The loss due to the imperfect clipping has also been estimated to be about 1% in Section 3.4.

As discussed in Sections 3.5 and 3.6, the loss due to imperfect data recording and reproducing has been estimated to be about 1%, and the loss accompanied with the correlation processing to be about 7.4%.

These results are summarized in Table 2. By the table, we can conclude that the total coherence loss caused by imperfect VLBI system is around 50%. This total loss will be confirmed by using a zero-baseline method and will be reported in another paper.

Table 2 Summary of the coherence loss caused by an imperfect VLBI system

loss factors	loss	reference
Imperfect receiving	0.6%	L_c given by Eq. (3.17)
Imperfect image rejection	4.5%	$1 - \beta_{ir}$ given by Eq. (3.18)
Imperfect filtering	3%	$1 - \beta_F\beta_R$ given by Eqs. (3.20) and (3.22) and Table 1
Imperfect sampling	36%	$1 - \beta_q$ given by Eq. (3.23)
	1%	$1 - \beta_c$ given by Eq. (3.24)
Imperfect data recording and reproducing	1%	$1 - \beta_{PER}$ given by Eq. (3.25) when $P_E = 10^{-3}$
Correlation processing	4%	$1 - \beta_{fr}$ given by Eq. (3.29)
	3.4%	$1 - \beta_{fb}$ given by Eq. (3.32)
Total loss	53.5%	

4. Coherence Loss due to phase fluctuations in atmosphere

In the preceding sections, we have discussed the coherence loss due to imperfectness of a VLBI system. In this section, we will consider the loss due to phase fluctuations in atmosphere.

The coherence function for the phase fluctuations in atmosphere is the same as that for the frequency instability expressed by Eq. (3.2), if we regard φ (t) in the equation as the phase fluctuations in atmosphere. Therefore, the only subject we should study is the statistics of the fluctuations. Since the statistical property may vary with time and may heavily depend on weather conditions, especially on humidity, it is difficult to give the statistics under every possible weather condition.

We have some models(13), however, which characterize the worst condition during warm, humid and cloudy weather, and the best condition during cool, dry and clear weather. We also have a experimental result obtained by using a real-time VLBI which has been performed since 1979 at 7.35-cm wavelength on a 47-km baseline(17). The result gives the statistics expressing actual situation.

In the experiments, strong noises from artificial satellites, i.e. a Japanese communications satellite (CS) and INTELSAT are received and processed by using a K-2 VLBI system(17). By using phase variations measured at different elevation angles, i.e., CS at about 48 deg and INTELSAT at about 2 deg, the Allan variance of the phase fluctuations in atmosphere has been empirically derived as

$$\sigma_\varphi^2 = 0.04\ \tau^{1.4\sim 2.8}[1/\sin(\mathrm{El})], \quad \ldots \quad (4.1)$$

where τ is the averaging time and El is the elevation angle. This can be converted into the equivalent frequency instability as

$$\sigma_y^2 = 2\times 10^{-26}\ \tau^{-0.6\sim 0.8} \quad \ldots \quad (4.2)$$

and is indicated by a shaded part bordered with two broken lines in Fig. 11.

As also shown in the figure, the square root of the Allan variance characterizing the models for the worst and the best conditions is constant up to a specific averaging time and goes down at a rate of τ^{-1} (11). Hence, for a typical condition in Japan, we will adopt a model shown by a heavy line in Fig. 11, taking approximately the central values of experimental results given by Eq. (4.2). In these models, the Allan variance is constant like a Flicker frequency noise up to a specific averaging time, and more than the averaging time it goes down at a rate of τ^{-2} like a white phase noise.

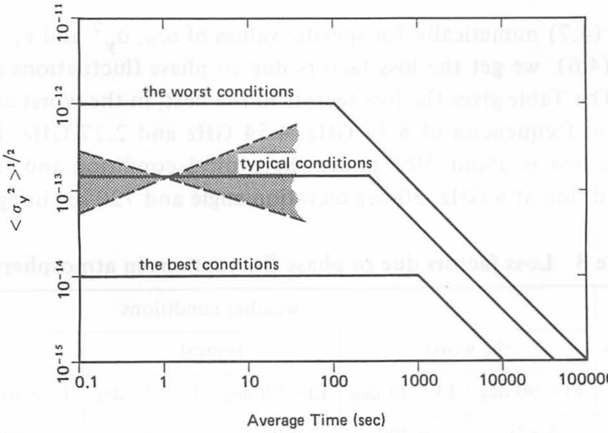

Fig. 11 Allan variance of phase fluctuations in atmosphere
The shaded part shows the experimental results by the K-2 VLBI system. The model for the typical conditions (straight lines) is typified from the experimental results.

According to the discussions in Section 3.1, the true variance can be written as

$$I^2(\tau) = \sigma_y^2/(2\ln 2)\ \ln(\tau_{max}/\tau) \quad \text{(4.3)}$$

for Flicker frequency noise and

$$I^2(\tau) = (2/3)\,\alpha_p \tau^{-2} \quad \text{(4.4)}$$

for the white phase noise. At the specific averaging time, τ_1, these two functions should be coincident. So an arbitrary parameter τ_{max} in Eq. (4.3) is fixed as

$$\tau_{max} = \tau_1 \exp\left[(4\ln 2/3)(\alpha_p/\sigma_y^2)\,\tau_1^{-2}\right] \quad \text{(4.5)}$$

Introducing Eqs. (4.3), (4.4), (4.5) into (3.3), we get the expected value of the coherence function for the estimation of the loss due to the phase fluctuations in atmosphere as

$$E\,[C^2(T)] = I(T; \omega_0, \sigma_y^2, \tau_1) + U(T - \tau_1)\,[(\tau_1/T) - 1]^2 \exp(-\omega_0^2 \sigma_y^2 \tau_1^2/3), \quad \text{(4.6)}$$

where T : integration time
ω_0 : observation frequency (= frequency of local oscillator)
σ_y^2 : constant Allan variance up to a specific averaging time of τ_1
τ_1 : transitional averaging time from constant to τ^{-1}

and $U(t)$ is a unit step function, $U(t) = 1$ at $t > 0$ and $U(t) = 0$ at $t < 0$, and $I(T; \omega_0, \sigma_y^2, \tau_1)$ is defined as

$$I(T) = (2/T)\int_0^{\tau_1} \exp\left[-a\tau^2 \ln(b/\tau)\right](1 - \tau/T)\,d\tau, \quad \text{(4.7)}$$

where $a = \omega_0^2 \sigma_y^2/(4\ln 2)$ and $b = 2.52\,\tau_1$.

Integrating Eq. (4.7) numerically for specific values of ω_0, σ_y^2 and τ_1, and introducing the result into Eq. (4.6), we get the loss factors due to phase fluctuations in atmosphere as shown in Table 3. The Table gives the loss factors in the best, in the worst and in the typical weather conditions at frequencies of 8.39 GHz, 4.54 GHz and 2.27 GHz. From the Table, we can see that the loss is about 50% under the typical condition and reaches over 80% under the worst condition at 8 GHz, 30-deg elevation angle and 720-sec integration.

Table 3 Loss factors due to phase fluctuations in atmosphere

Frequencies	Integration time (sec)	weather conditions					
		the worst		typical		the best	
		El = 90 deg	El = 30 deg	El = 90 deg	El = 30 deg	El = 90 deg	El = 30 deg
2.27 GHz	240	0.826	0.707	0.978	0.967	0.990	0.990
	720	0.756	0.588	0.964	0.933	0.989	0.989
4.54 GHz	240	0.565	0.446	0.946	0.906	0.990	0.989
	720	0.397	0.270	0.875	0.779	0.988	0.985
8.39 GHz	240	0.378	0.307	0.858	0.769	0.989	0.987
	720	0.222	0.179	0.678	0.535	0.982	0.974

As has been suggested in the reference[11], the lower observation frequency gives more favorable result in the loss in atmosphere but unfavorable result in the loss in ionosphere, and frequencies around 2 GHz give the optimum observations, where the total loss in atmosphere and ionosphere is about twice as much as that in atmosphere. Thus, from Table 3, we can conclude that if we could use observation bandwidth in S-band (around 2 GHz) as wide as that in X-band (around 8 GHz), the coherence loss will be improved up to 6% under the typical weather conditions at 30-deg elevation angle and for 720-sec integration, and the maximum sensitivity will be obtained. A wideband receiver at around 2 GHz is now under development, which uses two or three cooled FET amplifiers in tandem.

5. Estimation of the delay observation error

In Section 2, we have reviewed a VLBI observation and have seen that the delay observation error can be estimated through the SNR defined by system parameters and the improvement factor of bandwidth synthesis which depends only on the allocation of observation frequencies. In Sections 3 and 4, we have given the coherence loss, i.e., the deterioration of the SNR, due to imperfect receiving system and phase fluctuations in atmosphere.

In this section, we will give the estimation of the delay observation error in some concrete cases, 1) intercontinental VLBI experiments between Kashima and Owens Valley Radio Observatory (OVRO) where a 26-m and a 40-m antennas and the K-3 VLBI system are used; 2) domestic VLBI experiments between Kashima and Tsukuba, Geographical Survey Institute (GSI), where the 26-m and a 5-m antennas and the K-3 system are used; and 3) mobile VLBI experiments where the 26-m and a transportable 3-m antennas and a super-wide band receiver are used.

The 26-m antenna, the receiving system and the K-3 VLBI system are described in detail in the reference[2], the 40-m antenna, receiving system at OVRO are noted in the reference[18] and the 5-m antenna, receiving system at GSI in the reference[4]. The performances of these system are summarized in Table 4. The transportable system having the 3-m antenna is in a stage of conceptional planning at this time, but is expected to have the performance as also shown in Table 4.

Table 4 Performances of antenna-receiving system in various VLBI stations

Item		Kashima (RRL)	OVRO	Tsukuba (GSI)	transportable
Antenna diameter		26 m	40 m	5 m	3 m
Antenna efficiency	S	56.6%	40%	32%	50%
	X	45.2%	50%	61%	60%
Antenna gain	S	52.8 dB	55.5 dB	36.5 dB	34.1 dB
	X	63.2 dB	67.5 dB	50.7 dB	46.2 dB
System noise	S	170 K (FET)	80 K (cooled paramp)	160 K (cooled paramp)	120 K (cooled FET)
	X	160 K (cooled paramp)	160 K (paramp)	125 K (cooled paramp)	200 K (cooled FET)

The correlated flux of the radio sources for the error estimation of the intercontinental VLBI experiments are assumed to be 6.3 Jy which is average flux density of 13 sources taken from the reference[19]. They are weak but have no harmful structure for delay observation even on a very long baseline. The correlated flux for the domestic and mobile VLBI experiments is assumed to be 8.8 Jy which is average flux density of 14 strong sources taken from the reference[20]. They have some structure but not so harmful on delay observations with a baseline in moderate length. The positions and correlated flux density of these sources are listed in Table 5.

Table 5 Lists of radio sources commonly used in VLBI observations

(a) A 13-source list in the reference[19]

source	right ascension			declination			flux
4C 67.05	2 hr	24 min	42.900 sec	67°	8′	6.00″	1.9 Jy
3C 84	3	16	29.549	41	19	51.65	12.5
NRAO 150	3	55	45.238	50	49	20.08	5.5
3C 120	4	30	31.586	05	14	59.40	4.0
OJ 287	8	51	57.229	20	17	58.50	6.0
4C 39.25	9	23	55.294	39	15	23.73	7.5
3C 273	12	36	33.246	02	19	43.30	10.0
3C 279	12	53	35.833	–5	31	08.00	10.0
0Q 208	14	04	45.625	28	41	29.46	1.5
3C 345	16	41	17.635	39	54	10.97	4.5
PKS 2134+00	21	34	05.225	00	28	25.00	6.0
VRO 42.22.01	22	00	39.387	42	02	08.40	5.0
3C 454.3	22	51	29.535	15	52	54.25	8.0

(b) A 14-source list in the reference[20]

source	right ascension			declination			flux
3C 84	3 hr	16 min	29.545 sec	41°	19′	51.69″	25.8* Jy
DA 193	5	52	01.373	39	48	21.94	5.2
P0605-08	6	05	36.026	–8	34	19.27	4.5
OJ 287	8	51	57.230	62	28	38.94	4.7
4C 39.25	9	23	55.294	39	15	23.83	7.8
3C 273	12	26	33.246	02	19	43.47	18.8*
3C 279	12	53	33.834	–5	31	07.88	12.2
3C 345	16	41	17.640	39	54	10.99	6.8
NRAO 530	17	30	13.538	–13	02	45.93	5.1
P 1741-038	17	41	20.621	–3	48	49.01	5.6
OV-236	19	21	42.18	–29	20	24.9	6.8
3C 418	20	37	07.497	51	08	35.59	5.6
P2134+004	21	34	05.226	00	28	25.02	8.0
3C 454.3	22	51	29.534	15	52	54.18	6.3

* adjusted in the strength for 12-min. integration instead of 4-min integration

The integration time is assumed to be 4 minutes for the intercontinental VLBI experiments and 12 minutes for the domestic and mobile VLBI experiments. The integration time of the 12-minutes (or the three 4-minutes) is usually taken so as to make an efficient use of a magnetic tape which can store the data of 12-minutes in each track of 9200 feet.

The video bandwidth can be selected out of 4 MHz, 2 MHz, 1 MHz, 500 KHz, 250 KHz and 125 KHz in the K-3 system, but the bandwidth of 2 MHz is commonly used in VLBI for geodetic applications and is assumed in this paper.

Introducing these values into Eqs. (2.2) and (2.9), we get the SNR as shown in Table 6. This is the ideal estimate of the SNR in the case of perfect receiving, and will be deteriorated by a factor of 0.25 in X-band and 0.45 in S-band owing to the coherence loss due to system imperfectness (0.5) and due to phase fluctuations in atmosphere as discussed in Sections 3 and 4, and these values result in the actual SNR shown in Table 6.

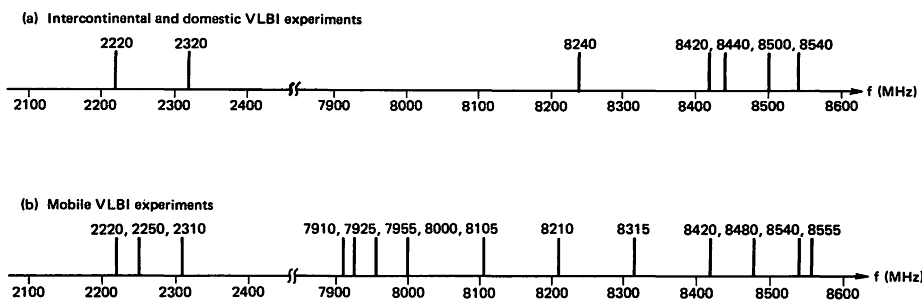

Fig. 12 Frequency arrangements of observing channels
(a) Intercontinental and domestic VLBI experiments
(b) Mobile VLBI experiments

The improvement factor defined in Section 2 depends on an arrangement of observation channels in each frequency band of S- and X-band. The arrangement of seven channels shown in Fig. 12 (a) is assumed for the intercontinental and the domestic experiments, and the arrangement of 14 channels shown in Fig. 12 (b) is assumed for the mobile experiments. Introducing frequencies of these channels into Eqs. (2.30) and (2.32), we get the improvement factor by bandwidth synthesis as shown in Table 6.

Substituting the final SNR and the improvement factor into Eqs. (2.27) and (2.33), we get the delay observation errors σ_τ in S-band and X-band as tabulated in Table 6.

The geometrical delay after correcting the ionospheric effect from the observations in S-band and X-band has an error given by[21]

$$\sigma_{\tau g} = \sqrt{\sigma_{\tau S}{}^2 + \alpha^4 \sigma_{\tau,X}{}^2}/(1 - \alpha^2), \qquad (5.1)$$

where τ_g is a geometrical delay observation error, $\sigma_{\tau,S}$ is the delay observation error in S-band, $\sigma_{\tau,X}$ is that in X-band, and α is a frequency ratio of the X-band to the S-band, which is about 4.

The geometrical delay observation errors are shown in the last column of Table 6, and are the final results concluded in this paper. The wording "geometrical", however, is not proper in strict meaning, because we need to consider many other factors which correct the observed delay in order to bring out the "purely geometrical delay". And we will suffer an increase in error by the additive corrections, but the consideration of those errors is beyond

Table 6 Delay observation error estimated in some concrete cases

Items	station (1) Kashima 26 m-	station (2) OVRO 40 m	station (1) Kashima 26 m-	station (2) Tsukuba 5 m	station (1) Kashima 26 m-	station (2) mobile 3 m
	S	X	S	X	S	X
Wave length: λ (m)	0.1322	0.0358	0.1322	0.0358	0.1322	0.0364
Antenna Gain of Stn (1): G1	1.91×10^5	2.09×10^6	1.91×10^5	2.09×10^6	1.91×10^5	2.02×10^6
Antenna Gain of Stn (2): G2	3.55×10^5	5.62×10^6	4.47×10^3	1.17×10^5	2.57×10^3	4.17×10^4
System Noise of Stn (1): T_{s1} (K)	170	160	170	160	170	160
System Noise of Stn (2): T_{s2} (K)	80	160	160	125	120	200
Source Intensity: S_c (W/m²/Hz)	6.3×10^{-26}	6.3×10^{-26}	8.8×10^{-26}	8.8×10^{-26}	8.8×10^{-26}	8.8×10^{-26}
Bandwidth: B (Hz)	2×10^6	2×10^6	2×10^6	2×10^6	2×10^6	2×10^6
Integration Time: T (sec)	240	240	240	240	720	720
T_{a1} from Eq. (2.2) (K)	0.606	0.487	0.847	0.680	0.847	0.679
T_{a2} (K)	1.13	0.0198	0.0198	0.0380	0.0114	0.0140
Ideal SNR from Eq. (2.9)	220	155	24.3	35.2	36.9	29.2
Loss in a system	0.5	0.5	0.5	0.5	0.5	0.5
Loss in atmosphere	0.97	0.77	0.97	0.77	0.94	0.54
Actual SNR	107	92.4	11.8	13.6	17.3	7.88
σ_{T1} Eq. (2.27) (nsec)	2.58	2.98	23.4	20.3	15.9	35.0
η Eq. (2.32)	123	400	123	400	131	1400
σ_T Eq. (2.33) (psec)	21.0	7.45	190	50.8	121	25.0
σ_{Tg} Eq. (5.1) (psec)	8.1		55.6		27.9	

the scope of this paper and will be given in another paper.

6. Conclusion

The delay observation error has been analyzed by many VLBI researchers. The author offers the error from another point of view and gives it in terms of the SNR in one observation channel and the improvement factor by bandwidth synthesis of several channels. We have seen that the SNR only depends on system parameters, such as antenna gain, receiving system noise, bandwidth of each observation channel, correlated flux density of source and integration time, whereas the improvement factor only depends on number and frequency allocation of the observation channels, that is, strategy of observations.

We have also seen that the SNR is reduced by some amount owing to imperfectness of receiving system and phase fluctuations in atmosphere. In this paper, much attention has been paied to the loss factors, especially to the loss due to phase fluctuations having Allan variance like a Flicker frequency noise, which is commonly observed in a typical hydrogen maser oscillator and in an atmospheric phenomenon.

As a result of the studies in this paper, the estimations of the delay observation errors are given for some concrete cases, and it has been concluded that the errors will be less than 0.1 nsec for all cases.

The work unfinished in this paper is the consideration for the effects of the source extent and of the polarization to calculate the SNR. The error estimations relating to the correction for the variation of atmospheric delay and cable delay to derive a "purely geometrical delay" is not also included. These subjects will be treated in another paper.

Acknowledgment

The work reported in this paper has been accomplished thanks to the previous work carried out by many VLBI researchers, who have started to study the VLBI and have made continuous efforts to its applications.

The author is also deeply indebted to Dr. N. Kawano and his colleagues for helpful discussions and encouragement.

He would like to thank Dr. N. Kawajiri and Prof. A. Tsuchiya for suggesting this problem and for stimulating interest in making it clear.

This work has been carried out for the development of the K-3 VLBI system and for the VLBI observations using this system. He also wishes to thank Dr. Y. Saburi, Dr. K. Yoshimura and Mr. F. Yamashita who have provided continuous support to the development of the VLBI system.

References

(1) Hinteregger, H.F., Shapiro, I.I., Robertson, D.S., Knight, C.A., Ergas, R.A., Whitney, A.R., Rogers, A.E.E., Moran, J.M., Clark, T.A., Burke, B.F.; "Precision Geodesy via Radio Interferometry", SCIENCE, **178**, 396-398, October 1972.

(2) Kawaguchi, N., Sugimoto, Y., Kuroiwa, H., Kondo, T., Hama, S., Amagai, J., Morikawa, T., Imae, M.; "The K-3 Hardware system being developed in Japan and its capability", NOAA Technical Report NOS 95 NGS 24, Proceedings of Symposium No. 5, IAG, Tokyo, 163-176, May 1982.

(3) Kawano, N., Takahashi, F., Yoshino, T., Koike, K., Kumagai, H., Kawajiri, N.; "Development of real-time VLBI and measurements of scintillation", J. Rad. Res. Labs., **29**, 127, 53-102, July 1982.

(4) Kawaguchi, N., Kawajiri, N., Kawano, N., Yoshimura, K., Ishii, H., Murakami, M., Nishimura, O., Yoshimura, Y., Kaidzu, M.; "A baseline determination between Kashima 26-m and Tsukuba 5-m antennas in joint VLBI experiment plan of RRL and GSI", NOAA Technical Report NOS 95 NGS 24, Proceedings of Symposium No. 5, IAG, Tokyo, 325-334, May 1982.

(5) Kraus, J.D., Radio Astronomy, Eq. (3.113) and Eq. (6.16), McGraw-Hill, 1966.

(6) Moran, J.M.; "Very Long Baseline Interferometric Observations and Data Reduction", Method of Experimental Physics, **12**, Part C: Radio Observations, p.228, edited by M.L. Leeks, Academic Press 1976.

(7) Whitney, A.R.; Precision geodesy and astrometry via Very-Long-Baseline Interferometry, Doctor Thesis at the Massachusetts Institute of Technology, Appendix E, January 1974.

(8) Rogers, A.E.E.; "Very Long Baseline Interferometry with large effective bandwidth for phase-delay measurements", Radio Science, **5**, 10, 1239-1247, October 1970.

(9) Whitney, A.R., Hinteregger, H.F., Knight, C.A., Levine, J.I., Lippincot, S., Clark, T.A., Shapiro, I.I., Robertson, D.S.; "A very-long-baseline interferometer system for geodetic applications", Radio Science, **11**, 5, 421-432, May 1976.

(10) Kawaguchi, N., Kawano, N.; "Bandwidth synthesis techniques for precise delay measurement in VLBI", Review of Rad. Res. Labs., **24**, 130, 539-549, September 1978 (in Japanese).

(11) Rogers, A.E.E.; "Coherence Limits for Very-Long-Baseline Interferometry", IEEE trans., **IM-30**, 4, 283–286, December 1981.
(12) Rutman, J.; "Characterization of Phase and Frequency Instabilities in Precision Frequency Sources: Fifteen Years Progress", Proc. IEEE, **66**, 9, 1048–1075, September 1978.
(13) Rogers, A.E.E.; "The sensitivity of a very long baseline interferometer", Radio Interferometry Techniques for Geodesy, NASA Conference Publication 2115, 1980.
(14) Whitney, A.R., Precision geodesy and astrometry via Very-Long Baseline Interferometry, Doctor Thesis at the Massachusetts Institute of Technology, section 3.3, p.99, January 1974.
(15) Whitney, A.R.; "Mark III correlator and software", ibid in the reference (13).
(16) Rogers, A.E.E.; "Broad-Band Passive 90° RC Hybrid with Low Component Sensitivity for Use in the Video Range of Frequencies", Proc. IEEE, **59**, 11, 1617–1618, November 1971.
(17) Kawano, N., Development of accurate very long baseline interferometer and measurement of scintillation, Doctor Thesis at Kyushu University, 1982.
(18) Rogers, A.E.E., *et al.*, Electronics Rack and Tape Recorder, Mark-III VLBI system documentation, Vol. **1**, January 1982.
(19) Ma, C., Very Long Baseline Interferometry Applied to Polar Motion, Relativity, and Geodesy, Doctor Thesis at University of Maryland, May 1978.
(20) Wu, S.C.; "Error Estimation for ORION Baseline Vector Determination", TDA Progress Report 42-57, March and April 1980.
(21) Shapiro, I.I., Estimation of Astrometric and Geodetic Parameters, Method of Experimental Physics, Vol. **12**, Part C: Radio Observations, p.261, edited by Meeks, M.L., Academic Press, 1976.

APPENDIX: Effect of statistical dependence between samples

Uncorrelated noise power increases as statistical dependence between samples increases, and has been given by Eq. (3.21) in section 3.3. Here the Eq. (3.21) is derived from Eq. (2.5) in section 2.

Expanding the expectation value of the products of four zero-mean Gaussian variables in the Eq. (2.5), we get

$$E\,[n_{1m}n_{2m}n_{1n}n_{2n}] = E\,[n_{1m}n_{2m}]\,E\,[n_{1n}n_{2n}] + E\,[n_{1m}n_{1n}]\,E\,[n_{2m}n_{2n}] + E\,[n_{1m}n_{2n}]\,E\,[n_{1n}n_{2m}] \quad \cdots\cdots \quad (A.1)$$

From the fact that n_1 (t) and n_2 (t) are statistically independent of each other, the right-hand side of the equation remains only the second term, and others becomes zero.

Introducing this into Eq. (2.5) and making rearrangement of the summations, we get

$$\begin{aligned} E\,[n_3\,\tau_i)^2] &= (1/N)^2 \sum_{m=1}^{N}\sum_{n=1}^{N} E\,[n_{1m}n_{1n}]\,E\,[n_{2m}n_{2n}] \\ &= (1/N)\left\{1+(2/N)\sum_{\tau=1}^{N}\sum_{m=1}^{N-\tau} E\,[n_{1m}n_{1m+\tau}]\,E\,[n_{2m}n_{2m+\tau}]\right\} \cdots\cdots \quad (A.2) \end{aligned}$$

Since it can be usually assumed that n_1 (t) and n_2 (t) are stationary random process,

$$E\,[n_{1m} n_{1m+\tau}] = R_{11}\,(\tau)$$

$$E\,[n_{2m} n_{2m+\tau}] = R_{22}\,(\tau), \qquad \text{(A.3)}$$

Eq. (A.2) can be rewritten as

$$E\,[n_3\,(\tau_i)^2] = (1/N)\,[1 + 2\sum_{\tau=1}^{N} W\,(\tau)\,R_{11}\,(\tau)\,R_{22}\,(\tau)]\,, \qquad \text{(A.4)}$$

where $W\,(\tau)$ is $(N - \tau)/N$ and becomes gradually smaller than unity as τ approaches to N, while $R_{11}\,(\tau)$ and $R_{22}\,(\tau)$ become rapidly smaller than unity. Thus the $W\,(\tau)$ can be approximated to unity, and the Eq. (3.21) is obtained.

It should be noted that the approximation is valid only when the inverse of a cut-off frequency of a filter is much less than the integration time. This condition on the cut-off frequency is satisfied for usual cases.